ACS central science

Research Article

Cite This: ACS Cent. Sci. 2018, 4, 543−547

Polymerization-Induced Self-Assembly of Micelles Observed by Liquid Cell Transmission Electron Microscopy

Mollie A. Touve,[†,∥,⊥] C. Adrian Figg,[#] Daniel B. Wright,[†,‡,§,∥] Chiwoo Park,[○] Joshua Cantlon,[▽] Brent S. Sumerlin,[*,#] and Nathan C. Gianneschi[*,†,‡,§,∥]

[†]Department of Chemistry, [‡]Department of Materials Science & Engineering, [§]Department of Biomedical Engineering, Northwestern University, Evanston, Illinois 60208, United States

[∥]Department of Chemistry & Biochemistry, [⊥]Department of NanoEngineering, University of California, San Diego, La Jolla, California 92093, United States

[#]George & Josephine Butler Polymer Research Laboratory, Center for Macromolecular Science & Engineering, Department of Chemistry, University of Florida, Gainesville, Florida 32611, United States

[○]Department of Industrial & Manufacturing Engineering, Florida State University, Tallahassee, Florida 32310, United States

[▽]SCIENION AG, Berlin 12489, Germany

Supporting Information

ABSTRACT: In this paper, we describe the use of liquid cell transmission electron microscopy (LCTEM) for inducing and imaging the formation of spherical micelles from amphiphilic block copolymers. Within the irradiated region of the liquid cell, diblock copolymers were produced which self-assembled, yielding a targeted spherical micellar phase via polymerization-induced self-assembly (PISA). Critically, we demonstrate that nanoparticle formation can be visualized in situ and that in the presence of excess monomer, nanoparticle growth occurs to yield sizes and morphologies consistent with standard PISA conditions. Experiments were enabled by employing automated LCTEM sample preparation and by analyzing LCTEM data with multi-object tracking algorithms designed for the detection of low-contrast materials.

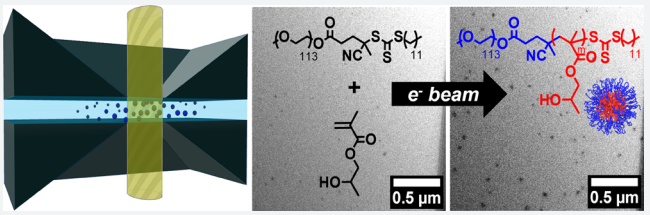

Dispersion polymerization-induced self-assembly (PISA) is a simple and robust approach for accessing amphiphilic materials with the benefit of obtaining targeted morphologies at high concentrations (10−50 wt %) and in a highly scalable fashion.[1−7] This approach is in contrast to the typical, two-step methods for preparing materials assembled from amphiphilic block copolymers, where the desired polymer is synthesized and then subsequently assembled by dissolution or gradual change of the solvent conditions.[8,9] In water, the PISA technique relies on chain-extension of a hydrophilic polymer with a water-soluble monomer that leads to the growth of a hydrophobic block. A homogeneous polymerization is initially achieved. However, as the second block becomes increasingly hydrophobic via chain extension, the block copolymers self-assemble into nanoparticles, and the polymerization transitions into a dispersion polymerization. A series of nanoparticle morphologies is formed according to the constantly changing packing parameter of growing chains, with micelles being the first morphology of the polymer self-assembly trajectory.[1]

Polymeric micelles are typically characterized by scattering methods, which provide averaged information for a sample within the bulk, with the data being fit to a determined model.[10,11] By contrast, high-resolution imaging methods such as cryogenic transmission electron microscopy are limited to capturing "snapshots" of soft nanomaterials frozen in time and provide insufficient temporal resolution.[12] Altogether, no broadly employed method provides direct information on a particle-by-particle basis in a native liquid environment.[13,14] However, liquid cell transmission electron microscopy (LCTEM) can potentially provide temporal and spatial insight into nanoscale phenomena.[13,15−20] Visualizing the progression of block copolymer self-assembly in real time would provide an opportunity to examine established theories of aggregation, reorganization, and morphological evolution to further understanding of how polymeric nanoparticles form under standard conditions.

While LCTEM imaging of the full range of morphologies formed during PISA is challenging within the subdiffusive environment of the liquid cell and during the drastic viscosity changes that generally occur during formation of anisotropic nanoparticles (e.g., worms), we reasoned that the first step in exploiting this technology to study PISA was to determine the feasibility of the electron beam for initiating polymerization to induce self-assembly. LCTEM is a nascent technique in development for observing dynamics and formation of a variety of materials, with the vast majority of studies being on inorganic systems.[21−26] Moreover, few reactions have been initiated in

Received: March 7, 2018
Published: April 25, 2018

DOI: 10.1021/acscentsci.8b00148
ACS Cent. Sci. 2018, 4, 543−547

the liquid cell and examined directly for soft, organic materials.[19,20,27−30] A rare example involved the thermally initiated (with a temperature-controlled liquid cell) formation of nanoscale colloidal covalent organic frameworks.[19] With this in mind, we set out to investigate the utility of LCTEM for a soft organic matter system, produced directly, in situ, via a widespread and highly useful reaction. Therefore, we examined initiating radical polymerizations and directly observing the solution self-assembly of block copolymer amphiphiles in real time.

We hypothesized that the electron beam of a transmission electron microscope (TEM) could be used to generate radicals to initiate polymerization while imaging in solution. We reasoned that the utility and ease of reversible addition−fragmentation chain-transfer (RAFT)-mediated PISA would make this system an optimal platform for determining if polymerization and self-assembly can be directly initiated and imaged by LCTEM. Our approach relied on an iniferter polymerization mechanism,[31] for which we observed that electron beam irradiation led to the visualization of particle formation during imaging of a solution of RAFT-generated polymer and a vinyl monomer in the absence of azo initiator, presumably from homolytic cleavage of the thiocarbonylthio group of the macro-chain transfer agent (macroCTA), leading to initiation of polymerization and subsequent self-assembly within the irradiated region. By contrast, regions of the liquid cell not directly irradiated and separated by a distance of at least 10 μm from an irradiated area did not result in particle self-assembly.

Previous literature has shown that when the electron beam interacts with a liquid sample during imaging by LCTEM, radiolysis of the species in solution occurs, generating radicals.[32−34] Therefore, the nature and concentration of radicals produced during an LCTEM experiment are important considerations, since high concentrations of radicals will affect the kinetics of polymerization and may give uncontrolled chain growth and morphology evolution that is inconsistent with a well-behaved PISA system. However, we reasoned that the chemistry could be controlled if (1) we work in low electron flux conditions, where electron flux is the number of electrons irradiating a unit area per second ($e^-/Å^2$ s), and (2) we work at a sufficiently high macroCTA concentration to favor: (i) preferential initiation from the carbon-centered radicals resulting from homolytic cleavage of the trithiocarbonate macroCTA and, (ii) degenerative chain transfer over uncontrolled conventional radical polymerization. In the discussion that follows, we demonstrate that under these experimental conditions, we directly observed the formation of micelles in solution via PISA.

TEM imaging in liquid was achieved using a liquid cell holder and chips having 30 μm × 200 μm viewing windows and 30 nm-thick silicon nitride membranes.[20] The electron flux used for imaging in these studies was in the range of 0.5 $e^-/Å^2$ s, and the concentration of the poly(ethylene glycol) macroCTA (referred to herein as the trithiocarbonate macroCTA) was significantly high so that the concentration of generated radicals within an irradiated region was greater than the expected concentration of any solvent radiolysis products (see Supporting Information for additional details). Thus, any radical polymerization which occurred should result primarily from homolytic cleavage of the trithiocarbonate macroCTA.

The low TEM contrast of these organic polymeric materials is a challenge when imaging in liquids because of the background scattering of the solvent. To address this, we utilized the sciTEM, an automated piezoelectric-actuated dispenser capable of depositing picoliter droplets of solution onto the surface of a commercial liquid cell chip in a predefined array (Figures 1 and S1, and Movie S1) to form consistently thin liquid layers with minimal scattering.[35] See Supporting Information for equipment description and videos.

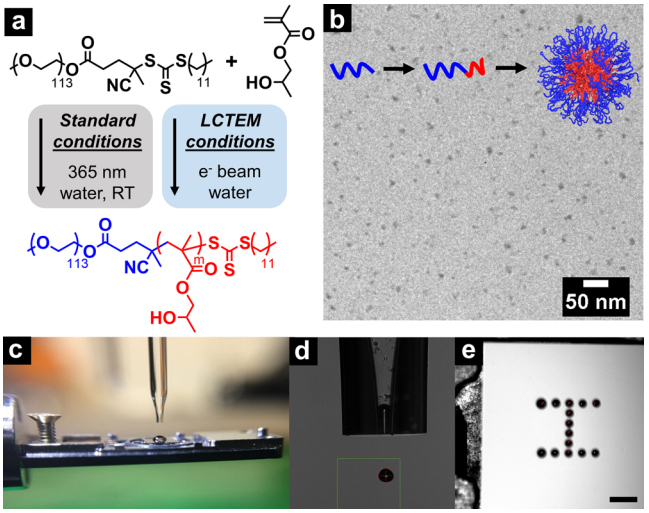

Figure 1. Polymers prepared, resulting assemblies, and LCTEM experimental setup. (a) Synthetic conditions for preparing diblock copolymers via either standard polymerization conditions (gray) or LCTEM irradiation (blue). (b) Uranyl acetate stained dry-state TEM image of spherical micelles formed through the polymerization-induced self-assembly of PEG-*b*-PHPMA diblock copolymers when performed under standard polymerization conditions, at a DP_n of the PHPMA block of 150. (c) A 0.5 μL droplet dispensed onto a bottom LCTEM chip. (d) An array of 300 pL droplets of solution containing HPMA and trithiocarbonate macroCTA being dispensed by the sciTEM. (e) Array of droplets on a bottom chip, scale bar = 200 μm.

First, we identified a proof-of-concept system where the polymers were expected to maintain core chain mobility while being hydrophobic enough for high TEM contrast. In these initial studies, micelles were prepared under standard polymerization conditions outside of the microscope via photo-PISA[2,36,37] chain-extension of the trithiocarbonate macroCTA with 2-hydroxypropyl methacrylate (HPMA). The PEG-*b*-PHPMA diblock copolymers assembled to yield spherical micelles as evidenced by dry-state TEM (Figure 1, and Figures S2−S5).

Initially, it was necessary to determine if the micelles formed under standard PISA conditions could be detected by LCTEM under reasonable electron fluxes and if the micelles grow when additional monomer is present in solution. A solution of HPMA and trithiocarbonate macroCTA was polymerized outside of the liquid cell via UV irradiation to yield PEG-*b*-PHPMA copolymers with a number-average degree of polymerization (DP_n) of the PHPMA block of 150 (see Supporting Information for details) to target the spherical micelle phase (Figure 1b). An additional 150 equiv of HPMA was added to the solution to chain-extend the core-forming PHPMA blocks and allow for micelle growth upon electron beam irradiation. This solution was briefly opened to air to both slow down polymerization kinetics and introduce molecular scavengers to potentially scavenge $OH^•$ radicals

DOI: 10.1021/acscentsci.8b00148
ACS Cent. Sci. 2018, 4, 543−547

and e^-_{aq}.[34] When this solution was initially imaged in the TEM, numerous particles 10−15 nm in diameter were present (Figures 2 and S6, and Movie S2). Particles attached to the

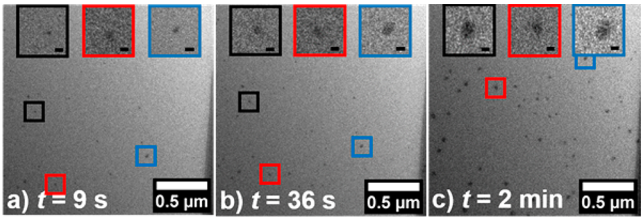

Figure 2. Direct observation of micelles within the liquid cell. (a−c) Snapshots taken during an LCTEM experiment of a solution of micelles that were initially formed outside of the microscope, under standard polymerization conditions, from HPMA and trithiocarbonate macroCTA, with an extra 150 equiv of HPMA added prior to imaging. The solution was continuously irradiated at 0.25 $e^-/Å^2$ s for 2 min. Insets are zoomed-in images of the particles boxed with the corresponding color. Scale bars of insets = 20 nm.

window could be tracked over time and were observed to increase in diameter to ∼25 nm during irradiation, demonstrating that spherical polymeric micelles can be observed in solution and grown via the PISA process in the presence of additional monomer using LCTEM. It is possible that the electron beam affects the livingness of the polymer chains, so we cannot assume that the PHPMA DP_n reached 300. In addition, the spatial confinement and reduced diffusion of species within the liquid cell may have limited the aggregation number of the micelles, resulting in the smaller micelle diameters observed during the LCTEM experiment.[38]

As controls, we tested these same imaging conditions and sequentially omitted one polymerization component from the solution. These controls included a solution containing only HPMA (no trithiocarbonate macroCTA) in water, to ensure that no particle formation was observed, and a solution of the macroCTA only, with no HPMA present. Each control solution was continuously irradiated at electron fluxes ranging from 0.1 to 1.7 $e^-/Å^2$ s at different regions of each liquid cell, for extended periods of time (>10 min). No structures formed in either case (Figures S7 and S8), with no observable change in the solution being imaged since both the trithiocarbonate and monomer are required for polymerization.

With these initial experiments in hand, we next aimed to observe the formation and growth of spherical micelles in the solution cell by TEM. In contrast to observing preformed micelles increasing in diameter (see above), this approach would allow the direct, real-time visualization of the particles as they assemble from the growing polymer amphiphiles in solution. Again, the automated approach was utilized to dispense solutions containing HPMA and the trithiocarbonate macroCTA into a liquid cell, followed by imaging under one of two different conditions: (1) by continuous imaging, wherein the sample was irradiated with the electron beam nonstop, and (2) by "pulsing" the sample with the beam,[19] wherein a 2 s exposure was taken to acquire a single snapshot image, followed by a dark period where the beam was turned off for 30 s. During the dark period, the electron beam does not provide energy to the system, and thus the energy dissipates. This process was repeated to obtain a time series of images. The goal of the pulsed conditions was to minimize potential sample damage from electron irradiation while providing enough energy to the system for sufficient radical formation for polymerization. In both cases, the samples were irradiated at a 0.45 $e^-/Å^2$ s flux. Automated multi-object tracking analysis (MOTA) developed for identifying and analyzing low-contrast particles in solution through the use of a background subtraction (BS) algorithm was applied to the raw LCTEM image series to track particles in each frame and monitor diameter changes as a function of time.[39,40] Growth profiles of the particles were generated by examining the final image of each sequence and identifying particles and recording their location and diameter. The location of each particle in the final image was used to "back-track" and identify the same particle in the previous image of the sequence. This process was reiterated back to the image in which the particle first appeared to generate a growth profile. See Supporting Information, Figure S9 for additional details on the BS and MOTA algorithms.

Under continuous imaging conditions, within ∼11 s of irradiation, particles began to form on the window of the liquid cell and grew over the course of 1 min (Figure S10 and Movie S3). The particles initially grew rapidly within 5 s of imaging, then equilibrated to an average diameter of 13 ± 3 nm (n = 11). Under pulsed imaging conditions, micelles began to form 80 s after the first exposure was taken, and micelle adhesion and growth were observed for up to 250 s after the first exposure (Figures 3 and S11). The micelles equilibrated to an average diameter of 13 ± 4 nm (n = 27). These diameters are similar to

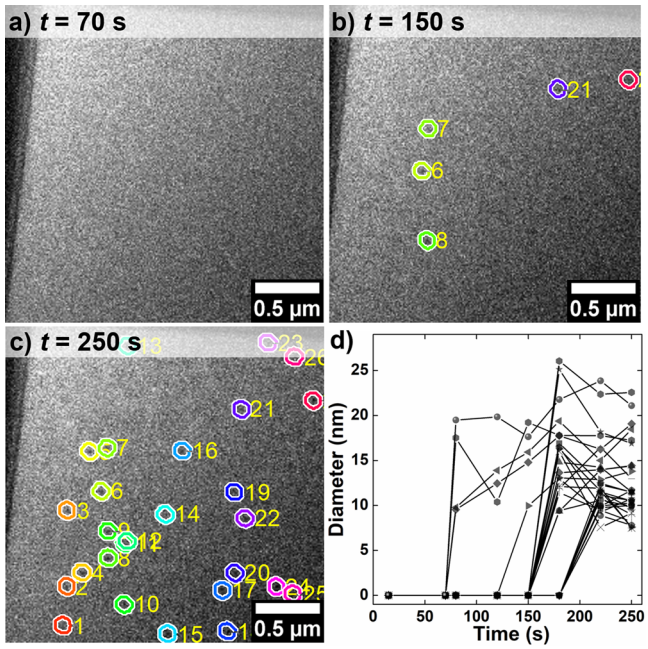

Figure 3. Tracking micelle growth during PISA by Multi-Object Tracking Analysis (MOTA) when the monomer solution is periodically exposed to the electron beam. (a−c) Images acquired over 5 min during the irradiation of a monomer solution of HPMA and macroCTA. The solution was "pulsed" with the electron beam for a 2 s exposure at 0.45 $e^-/Å^2$ s, and then the beam was turned off for 30 s. This process was repeated for 5 min. A multi-object tracking algorithm was applied to the images to detect particle locations and diameters. (d) Growth profile of micelle diameters, where each time point represents when the sample was pulsed with the electron beam to acquire an image. Note: Particles are numbered 1−27 (see also Supporting Information, Figure S11), in order of algorithm detection frame-by-frame.

DOI: 10.1021/acscentsci.8b00148
ACS Cent. Sci. 2018, 4, 543−547

one another, and importantly, they correspond to the particle diameters observed for standard solution preparations at the early stages of polymerization by dynamic light scattering (Figures 1b and S4). Again, it is possible that the electron beam affects the livingness of the polymer chains, so we cannot assume that the PHPMA DP_n reached 300, which may account for the smaller diameters observed. However, because the micelles forming under these different imaging conditions tend toward the same size, this suggests that the small micelle diameters may be because of limited aggregation numbers of the micelles, rather than the synthesis of polymers with lower DP_n. Further evidence of this micelle growth occurring via a PISA process includes how throughout imaging, numerous micelles were observed to suddenly appear at the window, while some disappeared back into solution, which suggests that PISA was not only occurring at the water−window interface, but also within the volume of the irradiated region of the liquid cell. Altogether, micelle growth does not appear to be significantly affected by the presence of the liquid cell window membrane.[41]

Finally, studies were performed to determine the electron flux threshold for imaging, as observed by obvious beam-induced damage (Figures S12 and S13, and Movie S4). These studies demonstrated that beam-induced effects which either altered the formation of the structures, their morphologies, or their interactions with each other or their environment, occurred at electron fluxes ∼10× higher than what was used in our imaging studies.

We have demonstrated that organic reactions, in this case polymerizations that induce micelle formation, can be directly initiated and visualized by LCTEM. Growth profiles of spherical micelles were determined through our background subtraction algorithm for identifying low-contrast particles against a solvent background,[39] and multi-object tracking analysis (MOTA) for automatically tracking multiple particles over image frames.[40] Furthermore, we determined that imaging samples at low electron fluxes in very thin liquid layers (∼100−500 nm) within the liquid cell are essential, and that pulsed imaging conditions are useful for controlling radical chemistry. These strategies may provide a path for observing the full gamut of possible morphological transitions that occur during PISA and, more generally, block copolymer solution self-assembly. To do so, particle size in the liquid cell and solution viscosity, specifically for the worm phase, must be considered. Moreover, analysis of the chemical species produced in the liquid cell is a topic of intense research, wherein very small quantities of material, polymers in this case, would need to be independently analyzed by a sensitive technique with high spatial resolution, at the end of the in situ TEM experiment. In short, continued innovation in new liquid cell design, experimental design, imaging conditions, and data analysis algorithms are needed to realize the full potential of this kind of dynamic videographic characterization of nanomaterials.

■ ASSOCIATED CONTENT

Supporting Information

The Supporting Information is available free of charge on the ACS Publications website at DOI: 10.1021/acscentsci.8b00148.

Experimental section, supporting Figures S1−S13, discussion on expected concentrations of radicals formed through TEM radiolysis, discussion on automated LCTEM sample deposition and chip placement; captions for Movies S1−S4 (PDF)

Movies S1 (AVI1), S2 (AVI2), S3 (AVI3), S4 (AVI4)

■ AUTHOR INFORMATION

Corresponding Authors

*(B.S.S.) E-mail: sumerlin@chem.ufl.edu.

*(N.C.G.) E-mail: nathan.gianneschi@northwestern.edu.

ORCID

C. Adrian Figg: 0000-0003-3514-7750

Brent S. Sumerlin: 0000-0001-5749-5444

Nathan C. Gianneschi: 0000-0001-9945-5475

Notes

No unexpected or unusually high safety hazards were encountered.

The authors declare no competing financial interest.

■ ACKNOWLEDGMENTS

This research was conducted with Government support under and awarded by DoD through the ARO (W911NF-17-1-0326), an ARO MURI (W911NF-15-1-0568), an AFOSR MURI (FA9550-16-1-0150), and an AFOSR National Defense Science and Engineering Graduate Fellowship, 32 CFR 168a, to M.A.T. We acknowledge the use of the UCSD Cryo-Electron Microscopy Facility, supported by NIH funding, to Dr. Timothy S. Baker and the Agouron Institute gifts to UCSD. This work also made use of the EPIC facility of Northwestern University's NUANCE Center, which has received support from the Soft and Hybrid Nanotechnology Experimental (SHyNE) Resource (NSF ECCS-1542205); the MRSEC program (NSF DMR-1720139) at the Materials Research Center; the International Institute for Nanotechnology (IIN); the Keck Foundation; and the State of Illinois, through the IIN. The algorithmic developments for the image background subtraction and multi-object tracking analysis were supported by NSF (CMMI-1334012) and AFOSR (FA9550-16-1-0110).

■ REFERENCES

(1) Warren, N. J.; Armes, S. P. Polymerization-Induced Self-Assembly of Block Copolymer Nano-Objects via RAFT Aqueous Dispersion Polymerization. *J. Am. Chem. Soc.* **2014**, *136* (29), 10174−10185.

(2) Tan, J.; Sun, H.; Yu, M.; Sumerlin, B. S.; Zhang, L. Photo-PISA: Shedding Light on Polymerization-Induced Self-Assembly. *ACS Macro Lett.* **2015**, *4* (11), 1249−1253.

(3) Canning, S. L.; Smith, G. N.; Armes, S. P. A Critical Appraisal of RAFT-Mediated Polymerization-Induced Self- Assembly. *Macromolecules* **2016**, *49*, 1985−2001.

(4) Figg, C. A.; Carmean, R. N.; Bentz, K. C.; Mukherjee, S.; Savin, D. A.; Sumerlin, B. S. Tuning Hydrophobicity To Program Block Copolymer Assemblies from the Inside Out. *Macromolecules* **2017**, *50*, 935−943.

(5) Wright, D. B.; Touve, M. A.; Adamiak, L.; Gianneschi, N. C. ROMPISA: Ring-Opening Metathesis Polymerization-Induced Self-Assembly. *ACS Macro Lett.* **2017**, *6*, 925−929.

(6) Wang, X.; Figg, C. A.; Lv, X.; Yang, Y.; Sumerlin, B. S.; An, Z. Star Architecture Promoting Morphological Transitions during Polymerization-Induced Self-Assembly. *ACS Macro Lett.* **2017**, *6* (4), 337−342.

(7) Figg, C. A.; Simula, A.; Gebre, K. A.; Tucker, B. S.; Haddleton, D. M.; Sumerlin, B. S. Polymerization-Induced Thermal Self-Assembly (PITSA). *Chem. Sci.* **2015**, *6* (2), 1230−1236.

(8) Choucair, A.; Eisenberg, A. Control of Amphiphilic Block Copolymer Morphologies Using Solution Conditions. *Eur. Phys. J. E: Soft Matter Biol. Phys.* **2003**, *10*, 37−44.
(9) Won, Y.-Y.; Davis, H. T.; Bates, F. S. Molecular Exchange in PEO - PB Micelles in Water. *Macromolecules* **2003**, *36*, 953−955.
(10) Kelley, E. G.; Murphy, R. P.; Seppala, J. E.; Smart, T. P.; Hann, S. D.; Sullivan, M. O.; Epps, T. H. Size Evolution of Highly Amphiphilic Macromolecular Solution Assemblies via a Distinct Bimodal Pathway. *Nat. Commun.* **2014**, *5*, 1−10.
(11) Patterson, J. P.; Robin, M. P.; Chassenieux, C.; Colombani, O.; O'Reilly, R. K. The Analysis of Solution Self-Assembled Polymeric Nanomaterials. *Chem. Soc. Rev.* **2014**, *43* (8), 2412−2425.
(12) Jain, S.; Bates, F. S. On the Origins of Morphological Complexity in Block Copolymer Surfactants. *Science* **2003**, *300*, 460−464.
(13) Parent, L. R.; Bakalis, E.; Ramírez-Hernández, A.; Kammeyer, J. K.; Park, C.; De Pablo, J.; Zerbetto, F.; Patterson, J. P.; Gianneschi, N. C. Directly Observing Micelle Fusion and Growth in Solution by Liquid-Cell Transmission Electron Microscopy. *J. Am. Chem. Soc.* **2017**, *139*, 17140−17151.
(14) Albertsen, A. N.; Szymanski, J. K.; Pérez-Mercader, J. Emergent Properties of Giant Vesicles Formed by a Polymerization-Induced Self-Assembly (PISA) Reaction. *Sci. Rep.* **2017**, *7*, 41534.
(15) Williamson, M. J.; Tromp, R. M.; Vereecken, P. M.; Hull, R.; Ross, F. M. Dynamic Microscopy of Nanoscale Cluster Growth at the Solid − Liquid Interface. *Nat. Mater.* **2003**, *2*, 532−536.
(16) de Jonge, N.; Ross, F. M. Electron Microscopy of Specimens in Liquid. *Nat. Nanotechnol.* **2011**, *6*, 695−704.
(17) Wright, D. B.; Patterson, J. P.; Pitto-Barry, A.; Lu, A.; Kirby, N.; Gianneschi, N. C.; Chassenieux, C.; Colombani, O.; O'Reilly, R. K. The Copolymer Blending Method: A New Approach for Targeted Assembly of Micellar Nanoparticles. *Macromolecules* **2015**, *48* (18), 6516−6522.
(18) Evans, J. E.; Jungjohann, K. L.; Browning, N. D.; Arslan, I. Controlled Growth of Nanoparticles from Solution with In Situ Liquid Transmission Electron Microscopy. *Nano Lett.* **2011**, *11*, 2809−2813.
(19) Smith, B. J.; Parent, L. R.; Overholts, A. C.; Beaucage, P. A.; Bisbey, R. P.; Chavez, A. D.; Hwang, N.; Park, C.; Evans, A. M.; Gianneschi, N. C.; Dichtel, W. R. Colloidal Covalent Organic Frameworks. *ACS Cent. Sci.* **2017**, *3*, 58−65.
(20) Patterson, J. P.; Abellan, P.; Denny, M. S.; Park, C.; Browning, N. D.; Cohen, S. M.; Evans, J. E.; Gianneschi, N. C. Observing the Growth of Metal−Organic Frameworks by in Situ Liquid Cell Transmission Electron Microscopy. *J. Am. Chem. Soc.* **2015**, *137* (23), 7322−7328.
(21) Williamson, M. J.; Tromp, R. M.; Vereecken, P. M.; Ross, F. M.; Hull, R. Dynamic Microscopy of Nanoscale Cluster Growth at the Solid − Liquid Interface. *Nat. Mater.* **2003**, *2*, 532−536.
(22) Nielsen, M. H.; Aloni, S.; De Yoreo, J. J. In Situ TEM Imaging of $CaCO_3$ Nucleation Reveals Coexistence of Direct and Indirect Pathways. *Science* **2014**, *345*, 1158−1162.
(23) Woehl, T. J.; Evans, J. E.; Arslan, I.; Ristenpart, W. D.; Browning, N. D. Direct in Situ Determination of the Mechanisms Controlling Nanoparticle Nucleation and Growth. *ACS Nano* **2012**, *6* (10), 8599−8610.
(24) Chee, S. W.; Tan, S. F.; Baraissov, Z.; Bosman, M.; Mirsaidov, U. Direct Observation of the Nanoscale Kirkendall Effect during Galvanic Replacement Reactions. *Nat. Commun.* **2017**, *8* (1), 1−8.
(25) Liao, H. G.; Zheng, H. Liquid Cell Transmission Electron Microscopy Study of Platinum Iron Nanocrystal Growth and Shape Evolution. *J. Am. Chem. Soc.* **2013**, *135*, 5038−5043.
(26) Abellan, P.; Parent, L. R.; Al Hasan, N.; Park, C.; Arslan, I.; Karim, A. M.; Evans, J. E.; Browning, N. D. Gaining Control over Radiolytic Synthesis of Uniform Sub-3-Nanometer Palladium Nanoparticles: Use of Aromatic Liquids in the Electron Microscope. *Langmuir* **2016**, *32* (6), 1468−1477.
(27) Evans, J. E.; Jungjohann, K. L.; Wong, P. C. K.; Chiu, P. L.; Dutrow, G. H.; Arslan, I.; Browning, N. D. Visualizing Macromolecular Complexes with in Situ Liquid Scanning Transmission Electron Microscopy. *Micron* **2012**, *43* (11), 1085−1090.
(28) Proetto, M. T.; Rush, A. M.; Chien, M. P.; Abellan Baeza, P.; Patterson, J. P.; Thompson, M. P.; Olson, N. H.; Moore, C. E.; Rheingold, A. L.; Andolina, C.; Millstone, J.; Howell, S. B.; Browning, N. D.; Evans, J. E.; Gianneschi, N. C. Dynamics of Soft Nanomaterials Captured by Transmission Electron Microscopy in Liquid Water. *J. Am. Chem. Soc.* **2014**, *136*, 1162−1165.
(29) Yamazaki, T.; Kimura, Y.; Vekilov, P. G.; Furukawa, E.; Shirai, M.; Matsumoto, H.; Van Driessche, A. E. S.; Tsukamoto, K. Two Types of Amorphous Protein Particles Facilitate Crystal Nucleation. *Proc. Natl. Acad. Sci. U. S. A.* **2017**, *114* (9), 2154−2159.
(30) Smeets, P. J. M.; Cho, K. R.; Kempen, R. G. E.; Sommerdijk, N. A. J. M.; De Yoreo, J. J. Calcium Carbonate Nucleation Driven by Ion Binding in a Biomimetic Matrix Revealed by in Situ Electron Microscopy. *Nat. Mater.* **2015**, *14* (4), 394−399.
(31) Carmean, R. N.; Becker, T. E.; Sims, M. B.; Sumerlin, B. S. Ultra-High Molecular Weights via Aqueous Reversible-Deactivation Radical Polymerization. *Chem.* **2017**, *2*, 93−101.
(32) Egerton, R. F.; Li, P.; Malac, M. Radiation Damage in the TEM and SEM. *Micron* **2004**, *35*, 399−409.
(33) Schneider, N. M.; Norton, M. M.; Mendel, B. J.; Grogan, J. M.; Ross, F. M.; Bau, H. H. Electron-Water Interactions and Implications for Liquid Cell Electron Microscopy. *J. Phys. Chem. C* **2014**, *118*, 22373−22382.
(34) Woehl, T. J.; Abellan, P. Defining the Radiation Chemistry during Liquid Cell Electron Microscopy to Enable Visualization of Nanomaterial Growth and Degradation Dynamics. *J. Microsc.* **2017**, *265* (2), 135−147.
(35) Patterson, J. P.; Parent, L. R.; Cantlon, J.; Eickhoff, H.; Bared, G.; Evans, J. E.; Gianneschi, N. C. Picoliter Drop-On-Demand Dispensing for Multiplex Liquid Cell Transmission Electron Microscopy. *Microsc. Microanal.* **2016**, *22* (3), 507−514.
(36) Tan, J.; Huang, C.; Liu, D.; Zhang, X.; Bai, Y.; Zhang, L. Alcoholic Photoinitiated Polymerization-Induced Self-Assembly (Photo-PISA): A Fast Route toward Poly(isobornyl Acrylate)-Based Diblock Copolymer Nano-Objects. *ACS Macro Lett.* **2016**, *5* (8), 894−899.
(37) Tan, J.; Liu, D.; Huang, C.; Li, X.; He, J.; Xu, Q.; Zhang, L. Photoinitiated Polymerization-Induced Self-Assembly of Glycidyl Methacrylate for the Synthesis of Epoxy-Functionalized Block Copolymer Nano-Objects. *Macromol. Rapid Commun.* **2017**, *38* (15), 1−7.
(38) Kröger, R.; Verch, A. Liquid Cell Transmission Electron Microscopy and the Impact of Confinement on the Precipitation from Supersaturated Solutions. *Minerals* **2018**, *8* (1), 21.
(39) Vo, G.; Park, C. Robust Regression For Image Binarization Under Heavy Noises and Nonuniform Background. *Pattern Recognition* **2018**, In press. https://doi.org/10.1016/j.patcog.2018.04.005.
(40) Park, C.; Woehl, T. J.; Evans, J. E.; Browning, N. D. Minimum Cost Multi-Way Data Association for Optimizing Multitarget Tracking of Interacting Objects. *IEEE Trans. Pattern Anal. Mach. Intell.* **2015**, *37* (3), 611−624.
(41) Jiang, N. Note on in Situ (Scanning) Transmission Electron Microscopy Study of Liquid Samples. *Ultramicroscopy* **2017**, *179*, 81−83.

DOI: 10.1021/acscentsci.8b00148
ACS Cent. Sci. 2018, 4, 543−547